

P-Stereogenic threonine derived Ir–P,N complexes. Reversible cyclometallation and asymmetric hydrogenation reactions

Pep Rojo^a, Agustí Lledós^b, Antoni Riera^{a,c,*}, Xavier Verdaguer^{a,c,*}

^a Institute for Research in Biomedicine (IRB Barcelona), The Barcelona Institute of Science and Technology, Baldri Reixac 10, Barcelona, E-08028, Spain

^b Departament de Química, Universitat Autònoma de Barcelona, Cerdanyola del Vallès, E-08193, Spain

^c Departament de Química Inorgànica I Orgànica, Secció de Química Orgànica. Universitat de Barcelona, Martí I Franquès 1, Barcelona, E-08028, Spain

ARTICLE INFO

Keywords:

P,N-ligands
P-Stereogenic phosphines
Iridium
Cyclometallation
Asymmetric hydrogenation

ABSTRACT

A threonine-derived phosphine-oxazoline iridium catalyst is reported, showcasing excellent selectivity in the hydrogenation of *N*-Boc-2,3-diarylallylamines. The reversible cyclometallation process between the square planar Ir(I) complex and the corresponding octahedral Ir(III) species is thoroughly investigated, while considering the influence of substitution at the phenyl group of the oxazoline on this equilibrium. X-Ray analysis reveals that the cyclometallated tridentate ligand adopts a *fac* coordination mode. Furthermore, the catalytic performance of these complexes in the asymmetric hydrogenation is evaluated and the utilization of Ir(III) pre-catalysts or Ir(I)/Ir(III) mixtures in hydrogenation reactions is proposed based on the observed equilibrium dynamics.

1. Introduction

Metal-catalyzed asymmetric hydrogenation plays a crucial role in organic synthesis by enabling the selective production of chiral compounds [1]. This powerful technique allows for the efficient preparation of pharmaceuticals, agrochemicals, and fine chemicals with high enantioselectivity, contributing to advancements in medicine, agriculture, and other industries. Iridium-catalyzed asymmetric hydrogenation exhibits unique features and advantages compared to rhodium and ruthenium catalysts [2]. Iridium catalysts demonstrate exceptional activity and selectivity in the hydrogenation of challenging substrates, such as unfunctionalized olefins [3], olefins with remote functional groups [4], and heteroaromatic compounds [5], providing access to a wide range of enantioenriched products.

As a result of our interest in the development of effective iridium catalysts for asymmetric hydrogenation [6], we have recently reported a threonine-derived P-stereogenic phosphine-oxazoline iridium catalyst that provided exceptional selectivity in the hydrogenation of *N*-Boc-2,3-diarylallylamines (Scheme 1a) [7]. The most successful catalyst contained a stereogenic *tert*-butylmethylphosphine moiety and a 3,5-di-*tert*-butylphenyl group directly attached to the oxazoline 2-position. Here we report on the reversible cyclometallation process occurring

between the square planar Ir(I) complex and the corresponding octahedral Ir(III) species, and how the substitution at the phenyl group of the oxazoline influences this equilibrium (Scheme 1b). The performance of these species in the asymmetric hydrogenation reaction is also described.

2. Results and discussion

Pre-ligands (*S*_P)-**3a** and (*R*_P)-**3a** were prepared according to the procedure described by our group [7], a five-step synthesis starting from L-threonine methyl ester hydrochloride and *tert*-butylmethyl phosphinous acid [8]. The key step in the synthesis is the stereo- and regioselective reaction of (*R*)- or (*S*)-*tert*-butylmethyl phosphinous mesylate with diaminoalcohol **1**, derived from threonine (Scheme 2). Benzoylation of the remaining amine functionality in **2** and cyclization afforded the corresponding phosphinooxazolines **3a** in good yields.

Coordination of pre-ligands **3a** to iridium was conducted in a three-step one-pot process (Scheme 3). Borane was removed with neat pyridine by heating at 90 °C overnight. After that, a solution of [Ir (cod) Cl]₂ (cod = 1,5-cyclooctadiene) in DCM was added to the free ligand. Addition of NaBAR₄ (sodium tetrakis [3,5-bis(trifluoromethyl)phenyl] borate) caused the abstraction of the chloride ligand and afforded

* Corresponding authors. Institute for Research in Biomedicine (IRB Barcelona), The Barcelona Institute of Science and Technology, Baldri Reixac 10, Barcelona E-08028, Spain.

E-mail addresses: antoni.riera@irbbarcelona.org (A. Riera), xavier.verdaguer@irbbarcelona.org (X. Verdaguer).

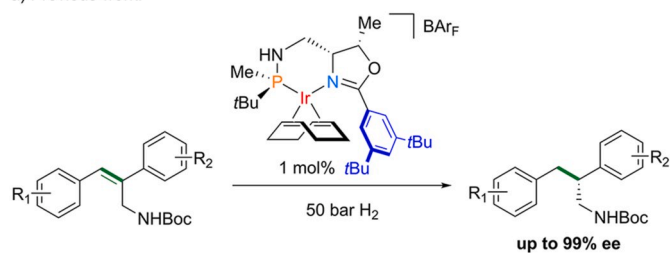
<https://doi.org/10.1016/j.tet.2023.133647>

Received 22 June 2023; Received in revised form 8 September 2023; Accepted 11 September 2023

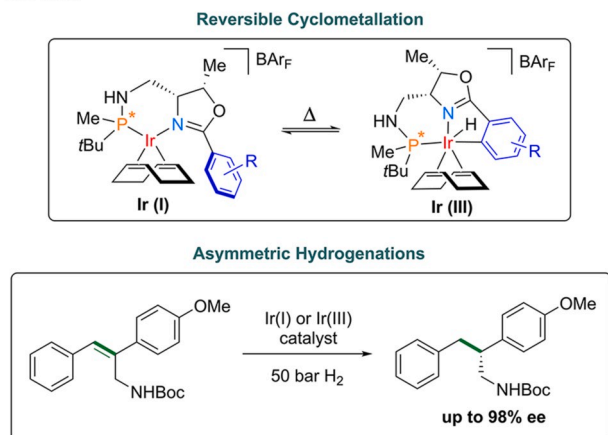
Available online 14 September 2023

0040-4020/© 2023 The Authors. Published by Elsevier Ltd. This is an open access article under the CC BY license (<http://creativecommons.org/licenses/by/4.0/>).

a) Previous work:



b) This work:



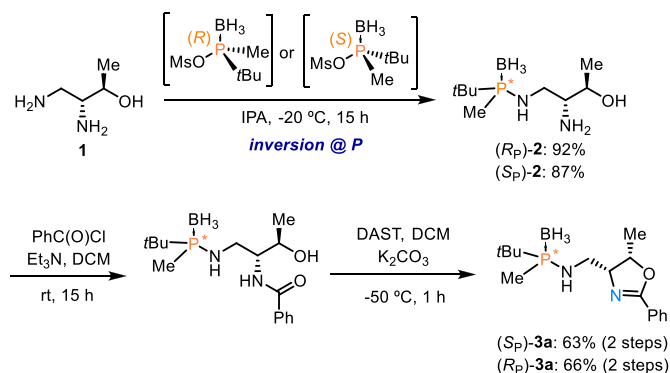
Scheme 1. a) Previous report of asymmetric hydrogenation of 2,3-diaryllallyl amines using a P-stereogenic P,N-iridium complex. b) Equilibrium of phenyl-substituted Ir(I) complex with the corresponding cyclometallated Ir(III) species and its use in hydrogenation reactions.

cationic complex (*R_p*)-**4a** in 73% yield. Initial analysis of (*R_p*)-**4a** by ¹H NMR revealed 2% of a by-product. This minor compound was identified as the Ir(III) complex (*R_p*)-**5a**, formed upon intramolecular C-metalation of the *ortho* carbon of the phenyl ring. ¹H NMR of complex (*R_p*)-**5a** shows a doublet (*J* = 13 Hz) at −14.92 ppm characteristic of a hydride bound to iridium and coupled to phosphorus in a *cis* position. At the

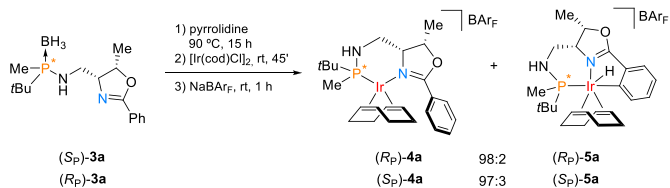
same time, the compound retains the characteristic resonances of the cod ligand. By evaporating a solution of the ligand and [Ir(cod)Cl]₂ before the addition of NaBAR_F, we could determine that cyclometallation already takes place in the neutral pentacoordinate intermediate complex of formula Ir(P,N)(cod)Cl, giving octahedral [IrH(P,N,C)(cod)]Cl by displacement of the chloride from the coordination sphere to the counterion position. Phosphine-borane (*R_p*)-**3a**, with opposite configuration at phosphorus, showed similar behavior and upon coordination to iridium and addition of NaBAR_F, the square-planar Ir(I) complex was isolated with 3% of the corresponding cyclometallated compound (*S_p*)-**5a**. When a solution of these mixtures in CDCl₃ was left at room temperature for several days, a slow evolution towards the corresponding cyclometallated species was observed by NMR (Fig. 1). In this case, complex (*R_p*)-**4a** evolved more rapidly than (*S_p*)-**4a**. After 5 days, 40% of complex (*R_p*)-**5a** was detected, while for the other diastereomer, only 25% of the cyclometallated (*S_p*)-**5a** was observed. It is worth to mention that due to the intramolecular nature of the C–H activation, transformation to the Ir(III) complex could be slowed down but not avoided when (*R_p*)-**4a** was kept as a solid in the freezer. Cyclometallated complexes **5a** could be isolated by silica flash chromatography as colorless solids and demonstrated to be stable at room temperature. In contrast, complexes **4a** were always isolated with small of amounts of the corresponding **5a** due to continuous isomerization [9].

In an attempt to increase the conversion towards the cyclometallated complex, a fresh batch of (*R_p*)-**4a** with minor impurities of (*R_p*)-**5a** was heated at 78 °C in CDCl₃ and the reaction monitored by ¹H NMR. After approximately 2 h of heating, the reaction reached a plateau at ~80% conversion and cyclometallation did not advance further after 24 h (Scheme 4a). This observation made us suspect that the Ir(I) and Ir(III) complexes could be in a reversible equilibrium. To further confirm this hypothesis, pure (*R_p*)-**5a** was heated at 78 °C for 2 h (Scheme 4b). Analysis by ¹H NMR revealed that (*R_p*)-**5a** had now evolved back to the square-planar complex, and the complexes (*R_p*)-**4a** and (*R_p*)-**5a** co-existed in a similar ratio to that observed when starting from the square-planar complex. This experiment confirmed that both species are indeed in equilibrium; while complex (*R_p*)-**5a** is more stable, the energy difference between both complexes is not large enough to completely shift the equilibrium towards the cyclometallated compound.

We next submitted (*R_p*)-**4a** to thermal equilibration in other solvents and temperatures (Table 1). While for 1,2-dichloroethane (DCE) at 78 °C and for THF at 100 °C the ratio of metalation was practically similar to CDCl₃ at 78 °C (Table 1, entries 1–3), the equilibrium was further shifted towards (*R_p*)-**5a** in toluene at 100 °C (Table 1, entry 4). We also studied the thermal equilibration in CDCl₃ at 78 °C of P-stereogenic threonine-derived complexes with other substituents in the oxazoline ring, to study the influence of structural factors in the equilibrium between **4** and **5**. The configuration of the phosphorus atom had a small effect on the position of the equilibrium; while equilibration of (*R_p*)-**4a**/**5a** produced a 20:80 mixture of complexes, the corresponding (*S_p*)-



Scheme 2. Synthesis of pre-ligands (*S_p*) and (*R_p*)-**3a**.



Scheme 3. Coordination of (*R_p*)- and (*S_p*)-**3a** to iridium and initial ratio of octahedral **5a**.

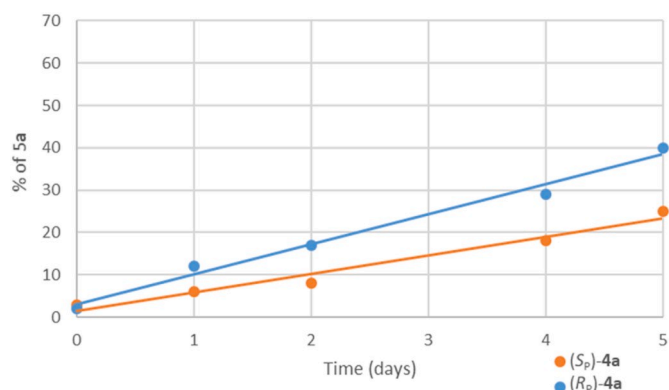
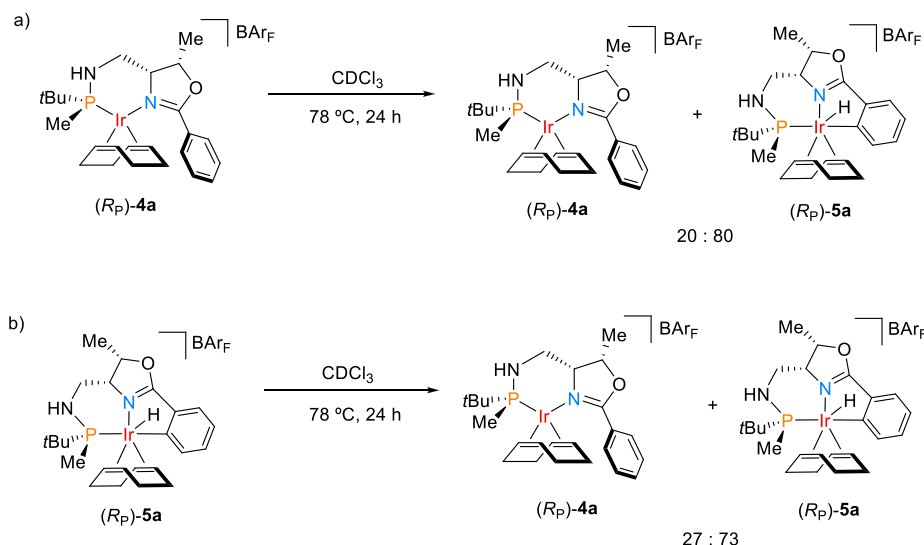


Fig. 1. Evolution of complexes (*R_p*)-**4a** and (*S_p*)-**4a** over time in CDCl₃ solution.



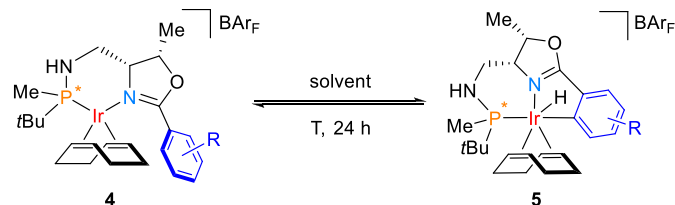
Scheme 4. Equilibration experiments upon thermal activation.

diastereomer gave a 10:90 mixture (Table 1, entries 1 and 5). Substitution of the aryl ring with electro-donating (2-Me) or electro-withdrawing groups (3,5-diF, 4- CF_3) caused no major changes in the equilibrium mixture, provided that a free *ortho* position was available for metalation (Table 1, entries 6–8). However, introduction of two methyl groups in *meta* position reverses the equilibrium mixture towards the square-planar complex (Table 1, entry 9). This fact can be attributed to the steric hindrance imposed by the methyl groups which hampers C–H activation and destabilize the corresponding cyclometallated **(Rp)-5e**. This trend is further confirmed by comparison with our previously reported compounds **(Rp)-4f** and **(Sp)-4f** bearing a 3,5-di-*tert*-butyl-phenyl moiety, which showed to be completely stable (Table 1, entries 10 and 11) [7]. It is worth noting that for complexes **5b–e**, minor amounts (5–21%) of other cyclometallated species could also be observed by ^1H NMR in the Ir–H region, which could be attributed to the formation of stereoisomeric coordination complexes.

In order to gather information about the structure of complexes **5a–e**,

Table 1

Influence of ligand structure on the equilibrium between square-planar and octahedral species.



Entry	Compounds	R	Solvent	T ($^\circ\text{C}$)	Ratio 4/5 ^a
1	(Rp)-4a/5a	H	CDCl_3	78	20:80
2	(Rp)-4a/5a	H	DCE	78	20:80
3	(Rp)-4a/5a	H	THF	100	23:77
4	(Rp)-4a/5a	H	Toluene	100	33:67
5	(Sp)-4a/5a	H	CDCl_3	78	10:90
6	(Rp)-4b/5b	3,5-diF	CDCl_3	78	15:85 ^b
7	(Rp)-4c/5c	2-Me	CDCl_3	78	12:88 ^b
8	(Rp)-4d/5d	4- CF_3	CDCl_3	78	6:94 ^b
9	(Rp)-4e/5e	3,5-diMe	CDCl_3	78	94:6 ^b
10	(Rp)-4f/5f	3,5-di- <i>t</i> Bu	CDCl_3	78	100:0 ^c
11	(Sp)-4f/5f	3,5-di- <i>t</i> Bu	CDCl_3	78	100:0 ^c

^a Ratio was determined by ^1H NMR analysis.

^b Minor amounts of other cyclometallated compounds were also observed.

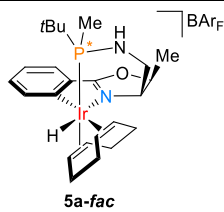
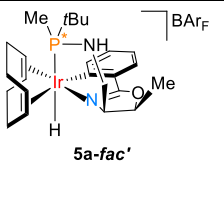
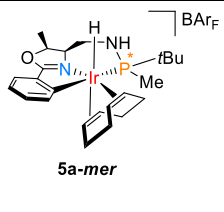
^c See reference 7.

we carried out computational studies of the relative energy of the three possible isomers that could be formed upon cyclometallation, for **(Rp)**- and **(Sp)-5a** (Table 2). For both diastereomers of **5a**, the calculations suggested isomer **5a-fac** as the more stable. In this complex, the P,N,C-ligand coordinates to the metal in a facial disposition. The difference in energy between **5a-fac** and the second more stable isomer, **5a-fac'**, is considerable ($\Delta G = 9.3$ kcal/mol for **(Rp)-5a** and 10.7 kcal/mol for **(Sp)-5a**). The meridional complex **5a-mer** was determined as the most unstable of the possible cyclometallated isomers. The high energetic difference between **5a-fac** and the other two possible isomers is in consonance with the highly stereoselective cyclometallation observed experimentally for most complexes.

To fully establish the structure and stereochemistry of cyclometallated compounds **5a–e** we sought to perform an X-ray analysis. For this purpose, suitable single crystals of **5c** were grown from DCM/hexane mixtures and diffracted. The resulting solid-state structure of **5c** is depicted in Fig. 2 [10]. The X-ray analysis demonstrates that, as suggested by the previous computational studies, the complex adopts an octahedral geometry as expected for iridium (III) complexes and that the P,N,C-ligand coordinates to the metal in a facial mode (*fac* isomer) instead of a meridional one. This is most likely due to the stereocenter in the oxazoline 4-position, which favors a non-flat disposition of the three atoms coordinated to iridium. The hydride is *trans* to the nitrogen atom of the oxazoline and *cis* to phosphorus, in agreement with the J coupling (13 Hz) observed for the Ir–H resonance. The cod ligand occupies the remaining coordination sites *trans* to both the phosphorus and the cyclometallated arene. We believe that the formation of cyclometallated species **5a–e** is the result of concerted oxidative addition of the aromatic C–H on the iridium center. NMR spectra of **5a** suggested there is no isomerization and that in solution cyclometallated compounds exist as *fac* isomers as in the solid state [11].

To assess the competence of both the Ir(I) and Ir(III) complexes as catalysts, we tested them in the asymmetric hydrogenation of allylamine **6** at 5 mol% under 50 bar of hydrogen pressure (Table 3). The use of catalyst **(Rp)-4a** short after its preparation, thus impurified with only 6% of the corresponding octahedral complex, provided 76% conversion and 94% ee (Table 3, entry 1). Upon heating to 80°C in DCE, full conversion was achieved with a slight decrease in selectivity (Table 1, entry 2). The corresponding diastereomer **(Sp)-4a**, again impurified with 8% of **(Sp)-5a**, proved to be more active and enantioselective, providing amine product with complete conversion and excellent 98% ee (Table 3, entry 3). This suggests that the Ir(III) complex does not interfere with the hydrogenation process. This result compares very favorably with the

Table 2Structure of the three possible isomers of **5a** and their computed relative Gibbs energies.

Configuration at P			
	5a-fac	5a-fac'	5a-mer
	ΔG (kcal/mol) ^a	ΔG (kcal/mol) ^a	ΔG (kcal/mol) ^a
(<i>R_P</i>)	0.0	9.3	11.7
(<i>S_P</i>)	0.0	10.7	17.6

^a) DLPNO-CCSD(T) Gibbs energies in chloroform solution at 25 °C. Details of the calculations as well as cartesian coordinates and 3D views of all the optimized structures can be found in the Supporting Information.

best catalyst of the series, (*S_P*)-**4f** (Table 3, entry 5). Under the same reaction conditions, we then tested the purified Ir(III) complexes (*R_P*)- and (*S_P*)-**5a**, which demonstrated to be inactive for the hydrogenation of the allyl amine (Table 3, entries 6 and 7). Analysis by ¹H NMR also confirmed that these cyclometallated complexes remained unchanged.

Iridium-catalyzed asymmetric hydrogenation of olefins takes place through an inner sphere mechanism, which involves direct binding of the metal and the substrate. In the activation of the square-planar Ir-P,N complex, H₂ binds to iridium and reduces the cyclooctadiene ligand, releasing cyclooctane and generating the active P,N-Ir(III) dihydride species. The inoperativeness of complexes **5a** in the hydrogenation reaction is attributable to the lack of free coordination sites to bind H₂ and release the cod ligand.

At this point we reasoned that we could take profit of the observed equilibrium between the cyclometallated Ir(III) species and the square-planar complexes. Running the hydrogenation at high temperature should enforce the transformation of complexes **5a** to the corresponding square-planar complexes, which are easily activated for hydrogenation. To demonstrate the viability of this process, we set up a hydrogenation at 80 °C in 1,2-dichloroethane using (*R_P*)-**5a** as a catalyst (Table 3, entry 8). Indeed, in this case we observed 70% conversion and 76% ee, which come close the values observed for (*R_P*)-**4a** in the same reaction conditions [12]. Unfortunately, the same hydrogenation reaction conditions with (*S_P*)-**5a** only yielded 36% conversion (Table 3, entry 9), much lower than that observed for square-planar (*S_P*)-**4a** at room temperature. In this case, analysis by ¹H NMR of the reaction crude revealed that an important quantity of octahedral catalyst had not been activated. This suggested that equilibration to the Ir(I) (*S_P*)-**4a** had not taken place, resulting in no activation of the catalyst. Equilibration experiments of

(*S_P*)-**5a** at 80 and 110 °C yielded only <1% and 5% respectively of the corresponding Ir(I) (*S_P*)-**4a** (Scheme 5). This indicates that for (*S_P*)-**5a**, the reductive elimination to yield back the square-planar complex has a considerably high energy barrier in comparison with (*R_P*)-**5a**.

Nevertheless, these experiments suggest that the existence of a reversible equilibration between the octahedral and the square-planar complexes allows the use of Ir(I)/Ir(III) mixtures or even Ir(III) pre-catalysts in hydrogenation reactions. A requirement for this strategy to succeed is a favorable kinetics between these two species for a fast equilibration towards the Ir(I) complex under hydrogenation reaction conditions.

3. Summary

In summary, we presented the development of a threonine-derived phosphine-oxazoline iridium catalyst and investigated the intriguing reversible cyclometallation process occurring between the square planar Ir(I) complex and the octahedral Ir(III) species. Furthermore, we explored the impact of various substituents on the oxazoline ring and their influence on the equilibrium between the two complexes. To gain insights into the structure of the cyclometallated complexes, we conducted X-ray analysis showing that the tridentate ligand adopts a *fac* coordination mode. Additionally, we assessed the catalytic performance of these complexes in the asymmetric hydrogenation of *N*-Boc 2-aryl-3-phenylallyl amine **6**, thereby highlighting the significance of the Ir(I)/Ir(III) equilibrium on catalytic activity.

4. Experimental section

General methods. All reactions were carried out in dried solvents under nitrogen atmosphere. Et₂O and DCM were dried and degassed in a solvent purification system (SPS PS-MD-3). Other commercially available reagents and solvents were used with no further purification. Employed methodologies that are described in the literature are duly cited. Unless otherwise specified, starting materials were obtained from commercial sources. Thin layer chromatography was carried out using TLC-aluminum sheets with silica gel. NMR spectra were recorded at 23 °C on a 400 MHz or 500 MHz apparatus. ¹H NMR and ¹³C NMR spectra were referenced either to relative internal TMS or to residual solvent peaks. ³¹P NMR spectra were referenced to phosphoric acid. Optical rotations were measured at room temperature (25 °C) and concentration is expressed in g/100 mL. Melting points were determined using a Büchi apparatus and were not corrected. IR spectra were recorded in a FT-IR apparatus. HRMS were recorded in a LC/MSD-TOF G1969A spectrometer using the nanoelectrospray technique. Hydrogenation reactions were carried out in a Büchi Glas Uster AG miniclave reactor. Calculation of the enantiomeric excess was carried out by HPLC techniques on an Agilent Technologies Series 1100 chromatograph with UV detector, by Enantia S.L.

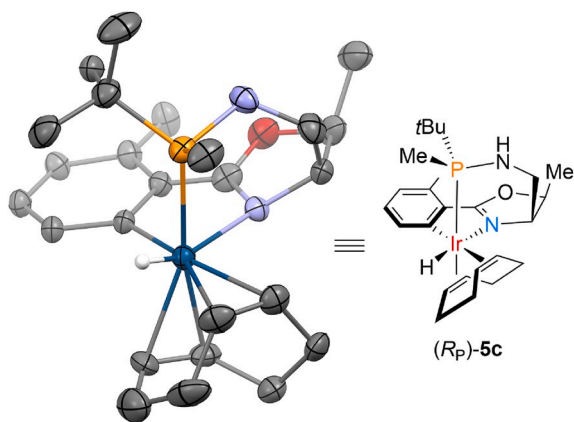
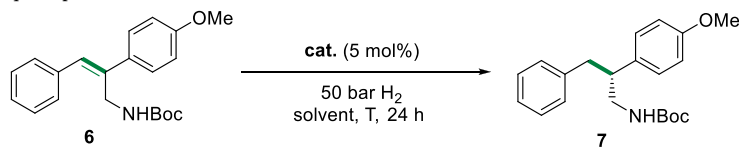
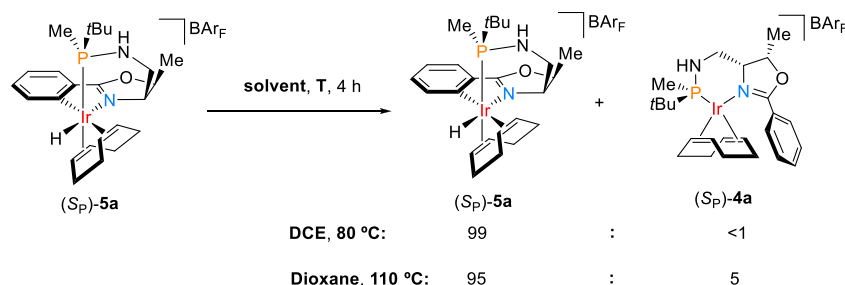


Fig. 2. X-Ray structure of (*R_P*)-**5c**. The ORTEP diagram shows ellipsoids at 50% probability. Only the H attached to the iridium center is shown. BARF counterion is omitted for clarity.

Table 3Asymmetric hydrogenation of **6** with square-planar **4a** and octahedral **5a**.

Entry	Catalyst	Solvent	Temperature	Conv (%)	ee (%) ^{a,b}
1	(<i>R_P</i>)- 4a ^c	DCM	rt	76	94
2	(<i>R_P</i>)- 4a	DCE	80	100	90
3	(<i>S_P</i>)- 4a ^d	DCM	rt	100	98
4	(<i>R_P</i>)- 4f	DCM	rt	100	88 ^e
5	(<i>S_P</i>)- 4f	DCM	rt	100	99 ^e
6	(<i>R_P</i>)- 5a	DCM	rt	0	–
7	(<i>S_P</i>)- 5a	DCM	rt	0	–
8	(<i>R_P</i>)- 5a	DCE	80	70	76
9	(<i>S_P</i>)- 5a	DCE	80	36	–

^a) Enantiomeric excess was determined by chiral HPLC.^b) The absolute configuration of **7** is (*R*) for all entries.^c) With 6% of the corresponding octahedral (*R_P*)-**5a**.^d) With 8% of the corresponding octahedral (*S_P*)-**5a**.^e) See reference 7.**Scheme 5.** Equilibration experiments upon thermal activation of (*S_P*)-**5a**.

Compounds **1**, **2**, **6** and (*R*)- or (*S*)-*tert*-butylmethyl phosphinous acid were prepared following previously described procedures by our group [7,13].

4.1. General procedure for the preparation of pre-ligands **3** (GP1)

To a solution of **2** (1 eq.) in DCM under inert atmosphere, Et₃N (2 eq.) was slowly added. The solution was then cooled down to 0 °C and the corresponding acid chloride (1 eq.) was added dropwise (if solid, dissolved in DCM). The reaction was left to stir at room temperature for 15 h. Then, HCl 1 M was added to the solution, the organic layer was separated and the aqueous phase was extracted twice with DCM. The combined extracts were dried over MgSO₄, filtered and concentrated under vacuum, obtaining intermediate amide without need of further purification. Consecutively, an oven-dried round-bottom flask was charged with the previous reaction crude (1 eq.), anhydrous K₂CO₃ (4 eq.) and dissolved in DCM. This solution was cooled down to –50 or –78 °C (depending on the solubility of the acylated product in DCM), a solution of DAST (2 eq.) in DCM was slowly added and the reaction was stirred at the same temperature for 1 h. Then, the reaction was quenched with saturated aqueous NaHCO₃, the mixture was warmed up to room temperature, the organic layer was separated and the aqueous phase was extracted twice with DCM. The combined extracts were dried over MgSO₄, filtered and concentrated under vacuum. The crude was purified by silica column chromatography using hexanes:EtOAc as eluent, affording the desired product.

4.2. Phosphinooxazoline (*S_P*)-**3a**

Following GP1, using (*S_P*)-**2a** (374.9 mg, 1.70 mmol), DCM (15 mL), Et₃N (0.48 mL, 3.41 mmol) and benzoyl chloride (0.20 mL, 1.70 mmol) afforded intermediate amide as a white solid (486.3 mg, 91% yield). ¹H NMR (400 MHz, CDCl₃) δ: 0.03–0.91 (m, BH₃), 1.13 (d, *J* = 14.1 Hz, 9H), 1.21 (d, *J* = 9.0 Hz, 3H), 1.26 (d, *J* = 6.5 Hz, 3H), 1.97 (br s, 1H), 3.20–3.40 (m, 2H), 3.99 (q, *J* = 7.6 Hz, 1H), 4.13–4.19 (m, 1H), 6.71 (br s, 1H), 7.41–7.48 (m, 2H), 7.49–7.54 (m, 1H), 7.77–7.91 (m, 2H) ppm.

Consecutively, following GP1, the obtained amide intermediate (350 mg, 1.08 mmol), K₂CO₃ (596.8 mg, 4.32 mmol), DCM (13.5 mL) and DAST (366.4 mg, 2.16 mmol) were used. Purification by silica column chromatography (hexanes:EtOAc 7:3) afforded (*S_P*)-**3a** as a white solid (229.3 mg, 69% yield). M. p.: 78–81 °C. [α]_D: +96.8 (c 0.84, CHCl₃). IR (ATR-FTIR) ν_{max}: 3359, 2958, 2925, 2855, 2363, 2339, 1646 cm^{–1}. ¹H NMR (400 MHz, CDCl₃) δ: 0.05–0.90 (m, BH₃), 1.17 (d, *J_P* = 14.0 Hz, 9H), 1.32 (d, *J_P* = 9.0 Hz, 3H), 1.39 (d, *J* = 6.7 Hz, 3H), 2.09 (br s, 1H), 3.01–3.12 (m, 1H), 3.22–3.34 (m, 1H), 4.24 (td, *J* = 9.1, 4.4 Hz, 1H), 4.90 (dq, *J* = 9.6, 6.7 Hz, 1H), 7.35–7.45 (m, 2H), 7.45–7.54 (m, 1H), 7.90–8.00 (m, 2H) ppm. ¹³C NMR (101 MHz, CDCl₃) δ: 9.9 (d, *J_P* = 37.7 Hz, CH₃), 15.1 (CH₃), 24.8 (3xCH₃), 29.9 (Cq), 31.0 (d, *J_P* = 40.7 Hz, Cq), 43.8 (CH₂), 69.5 (CH), 127.8 (CH), 128.4 (2xCH), 128.5 (2xCH), 131.7 (CH), 164.3 (Cq) ppm. ³¹P NMR (162 MHz, CDCl₃) δ: 69.4–71.5 (m) ppm. HRMS (ESI): calc for [C₁₆H₂₈BN₂OP + H]⁺: 307.2105, found 307.2115.

4.3. Phosphinoxazoline (R_p)-**3a**

Following GP1, using (R_p)-**2a** (79.4 mg, 0.36 mmol), DCM (2.8 mL), Et₃N (0.10 mL, 0.72 mmol) and benzoyl chloride (42 μ L, 0.36 mmol) afforded intermediate (R_p)-amide as a white solid (110.8 mg, 95% yield). ¹H NMR (400 MHz, CDCl₃) δ : 0.08–0.93 (m, BH₃), 1.10 (d, J = 14.1 Hz, 9H), 1.25 (d, J = 6.5 Hz, 3H), 1.35 (d, J = 9.2 Hz, 3H), 1.98 (br s, 1H), 3.07–3.37 (m, 2H), 3.79–3.98 (m, 1H), 4.29 (q, J = 6.5 Hz, 1H), 6.66 (d, J = 8.6 Hz, 1H), 7.41–7.48 (m, 2H), 7.48–7.56 (m, 1H), 7.77–7.82 (m, 2H) ppm.

Consecutively, following GP1, the obtained amide intermediate (110.8 mg, 0.34 mmol), K₂CO₃ (189 mg, 1.37 mmol), DCM (2.6 mL) and DAST (116 mg, 0.68 mmol) were used. Purification by silica column chromatography (hexanes:EtOAc 8:2) afforded (R_p)-**3a** as a colourless oil (229.3 mg, 69% yield). [α]_D: +120.8 (c 1.12, CHCl₃). IR (ATR-FTIR) ν_{max} : 3327, 2924, 2867, 2383, 1633 cm⁻¹. ¹H NMR (400 MHz, CDCl₃) δ : 0.11–0.88 (m, BH₃), 1.12 (d, J = 13.9 Hz, 9H), 1.35 (d, J = 8.4 Hz, 3H), 1.37 (d, J = 6.4 Hz, 3H), 2.22 (d, J = 9.5 Hz, 1H), 2.86–3.09 (m, 1H), 3.26–3.48 (m, 1H), 4.22 (td, J = 9.4, 4.1 Hz, 1H), 4.89 (dq, J = 9.4, 6.7 Hz, 1H), 7.36–7.44 (m, 2H), 7.45–7.52 (m, 1H), 7.91–7.96 (m, 2H) ppm. ¹³C NMR (101 MHz, CDCl₃) δ : 10.4 (d, J = 39.9 Hz, CH₃), 14.9 (s, CH₃), 24.8 (d, J = 3.0 Hz, 3xCH₃), 31.4 (d, J = 38.7 Hz, Cq), 44.4 (s, CH₂), 70.1 (d, J = 5.5 Hz, CH), 78.2 (CH), 127.9 (s, Cq), 128.3 (s, 2xCH), 128.5 (s, 2xCH), 131.6 (s, CH), 164.2 (s, Cq) ppm. ³¹P NMR (162 MHz, CDCl₃) δ : 68.69–72.37 (m) ppm. HRMS (ESI): calc for [C₁₆H₂₈BN₂OP + H]⁺: 307.2105, found 307.2111.

4.4. General procedure for the preparation of catalysts **4** (GP2)

The corresponding phosphine-borane (1 eq.) was added to a flame-dried Schlenk round-bottom flask, purged with vacuum-nitrogen cycles and dissolved in freshly distilled and degassed pyrrolidine (0.06 M). The mixture was stirred for 15 h at 90 °C. Then, under strict inert atmosphere, pyrrolidine was removed under vacuum and further dried at 50 °C for 30 min. A solution of [Ir(cod)Cl]₂ (0.05 eq.) in DCM was added to the free ligand and stirred at room temperature for 40 min. NaBARf (1 eq.) was then added and the solution was stirred for 1 h at room temperature. The resulting crude was purified by filtering through a plug of silica gel under nitrogen, eluting with hexanes:DCM 1:1 (the plug was initially washed with anhydrous Et₂O). The coloured fraction was collected and concentrated affording the desired product.

4.5. Complex (R_p)-**4a**

Following GP2, using (S_p)-**3a** (50 mg, 0.16 mmol), pyrrolidine (2.7 mL), [Ir(cod)Cl]₂ (55 mg, 0.08 mmol), DCM (2.7 mL) and NaBARf (149 mg, 0.16 mmol) afforded (R_p)-**4a** as an orange solid (174 mg, 73% yield). ¹H NMR (400 MHz, CDCl₃) δ : 1.05 (d, J = 15.0 Hz, 9H), 1.36 (d, J = 8.1 Hz, 3H), 1.41 (d, J = 6.7 Hz, 3H), 1.50–1.68 (m, 2H), 1.75–1.91 (m, 1H), 2.07–2.25 (m, 3H), 2.33 (dd, J = 16.8, 10.5, 6.5 Hz, 1H), 2.45–2.57 (m, 2H), 3.16–3.28 (m, 1H), 3.40–3.54 (m, 1H), 3.61–3.76 (m, 2H), 4.36–4.41 (m, 1H), 4.41–4.48 (td, J = 8.4, 3.9 Hz, 1H), 4.77–4.84 (m, 1H), 4.99–5.10 (m, 1H), 7.53 (s, 4H), 7.56 (t, J = 7.9 Hz, 2H), 7.68–7.73 (m, 1H), 7.71 (br s, 8H), 8.60–8.64 (m, 2H) ppm. HRMS (ESI, infusion): calc for [C₂₄H₃₇IrN₂OP]⁺: 593.2261, found 593.2265. Calc for [C₃₂H₁₂BF₂₄]⁺: 863.0660, found 863.0690. The compound was not further characterized due to its continuous isomerization to the cyclometallated species.

4.6. Complex (S_p)-**4a**

Following GP2, using (R_p)-**3a** (50.5 mg, 0.16 mmol), pyrrolidine (2.8 mL), [Ir(cod)Cl]₂ (55.4 mg, 0.08 mmol), DCM (2.8 mL) and NaBARf (151 mg, 0.16 mmol) afforded (S_p)-**4a** as an orange solid (144 mg, 60% yield). ¹H NMR (400 MHz, CDCl₃) δ : 1.08 (d, J = 14.9 Hz, 9H), 1.34 (dd, J = 6.5, 0.8 Hz, 3H), 1.39 (d, J = 6.7 Hz, 3H), 1.45–1.53 (m, 1H),

1.59–1.71 (m, 1H), 1.77–1.88 (m, 1H), 1.99 (br s, 1H), 2.07–2.18 (m, 1H), 2.18–2.37 (m, 3H), 2.40–2.55 (m, 1H), 3.23–3.45 (m, 1H), 3.68 (p, J = 7.0 Hz, 1H), 3.77–3.90 (m, 1H), 4.14–4.25 (m, 1H), 4.29 (dd, J = 10.0, 4.9, 2.4 Hz, 1H), 4.81 (br s, 1H), 4.88 (s, 1H), 5.11 (dq, J = 9.9, 6.7 Hz, 1H), 7.52 (s, 4H), 7.57 (t, J = 7.8 Hz, 2H), 7.70 (br s, J = 2.1 Hz, 8H), 7.70–7.74 (m, 1H), 8.76 (d, J = 8.2 Hz, 2H) ppm. HRMS (ESI, infusion): calc for [C₂₄H₃₇IrN₂OP]⁺: 593.2261, found 593.2263. Calc for [C₃₂H₁₂BF₂₄]⁺: 863.0660, found 863.0668. The compound was not further characterized due to its continuous isomerization to the cyclometallated species.

4.7. Complex (R_p)-**5a**

A 1:1 mixture of square-planar (R_p)-**4a** and octahedral (R_p)-**5a** complexes (72.1 mg, 0.050 mmol) was dissolved in CHCl₃ (4 mL) and heated at 78 °C for 2 h. After that, the solvent was evaporated and the resulting crude was purified by filtering through a plug of silica gel under nitrogen, eluting with anhydrous THF (the plug was initially washed with anhydrous Et₂O). In this way, the remaining square-planar complex could be eliminated, affording (R_p)-**5a** as a white solid (43.6 mg, 60% yield). [α]_D: +38.4 (c 0.42, CHCl₃). IR (ATR-FTIR) ν_{max} : 2953, 2922, 2851, 1607, 1468, 1352, 1270, 1119 cm⁻¹. ¹H NMR (400 MHz, CDCl₃) δ : -14.92 (d, J = 12.8 Hz, 1H), 0.60 (d, J = 16.4 Hz, 9H), 1.29 (d, J = 6.1 Hz, 3H), 1.56 (d, J = 6.7 Hz, 3H), 2.02–2.13 (m, 1H), 2.23–2.40 (m, 2H), 2.47–2.63 (m, 2H), 2.71–2.83 (m, 2H), 2.83–2.93 (m, 1H), 3.03–3.17 (m, 1H), 3.27–3.46 (m, 2H), 4.53–4.60 (m, 1H), 4.65–4.77 (m, 2H), 4.94–5.07 (m, 1H), 5.27–5.40 (m, 1H), 7.11 (td, J = 7.5, 1.1 Hz, 1H), 7.23–7.30 (m, 1H), 7.48 (dd, J = 7.7, 1.5 Hz, 4H), 7.53 (s, 1H), 7.70 (m, 9H) ppm. ¹³C NMR (101 MHz, CDCl₃) δ : 11.3 (d, J_p = 28.1 Hz, CH₃), 15.2 (CH₃), 25.0 (d, J_p = 3.7 Hz, 3xCH₃), 28.1 (CH₂), 31.2 (CH₂), 31.8 (d, J_p = 5.3 Hz, CH₂), 33.1 (d, J_p = 41.5 Hz, Cq), 35.2 (CH₂), 41.0 (d, J_p = 3.1 Hz, CH₂), 62.2 (CH), 81.6 (CH), 83.0 (CH), 89.7 (CH), 93.9 (d, J_p = 16.7 Hz, CH), 98.9 (d, J_p = 10.0 Hz, CH), 117.6 (4xCH), 124.3 (CH), 124.7 (q, J_F = 272.5 Hz, 8xCF₃), 128.6–129.4 (m, 8xCq), 128.8 (CH), 130.2 (CH), 134.8 (CH), 134.9 (8xCH), 141.9 (CH), 152.9 (d, J_p = 6.7 Hz, Cq), 161.8 (d, J_F = 50.0 Hz, 4xCq), 180.8 (Cq) ppm. ³¹P NMR (162 MHz, CDCl₃) δ : 48.6 (s) ppm. HRMS (ESI, infusion): calc for [C₂₄H₃₇IrN₂OP]⁺: 593.2261, found 593.2261. Calc for [C₃₂H₁₂BF₂₄]⁺: 863.0660, found 863.0655.

4.8. Complex (S_p)-**5a**

A 58:42 mixture of square-planar (S_p)-**4a** and octahedral (S_p)-**5a** complexes (107.0 mg, 0.074 mmol) was dissolved in CHCl₃ (6.1 mL) and heated at 78 °C for 2 h. After that, the solvent was evaporated and the resulting crude was purified by filtering through a plug of silica gel under nitrogen, eluting with anhydrous THF (the plug was initially washed with anhydrous Et₂O). In this way, the remaining square-planar complex could be eliminated, affording (S_p)-**5a** as a white solid (81.1 mg, 76% yield). [α]_D: +21.8 (c 0.99, CHCl₃). IR (ATR-FTIR) ν_{max} : 2953, 2928, 2902, 2875, 2850, 1608, 1437, 1353, 1271, 1105 cm⁻¹. ¹H NMR (400 MHz, CDCl₃) δ : -15.02 (d, J = 13.5 Hz, 1H), 0.58 (d, J = 8.9 Hz, 3H), 0.96 (d, J = 15.6 Hz, 9H), 1.55 (d, J = 5.4 Hz, 3H), 2.06–2.17 (m, 1H), 2.29–2.39 (m, 1H), 2.41–2.53 (m, 2H), 2.55–2.69 (m, 2H), 2.72 (q, J = 7.1 Hz, 2H), 3.18–3.28 (m, 1H), 3.29–3.41 (m, 1H), 3.55–3.63 (m, 1H), 4.44–4.54 (m, 1H), 4.96–5.02 (m, 1H), 5.08–5.16 (m, 1H), 5.16–5.23 (m, 1H), 5.28–5.36 (m, 1H), 7.14 (td, J = 7.6, 1.0 Hz, 1H), 7.21–7.26 (m, 1H), 7.50 (dd, J = 7.7, 1.5 Hz, 1H), 7.52 (s, 4H), 7.61 (d, J = 7.6 Hz, 1H), 7.69–7.71 (m, 8H) ppm. ¹³C NMR (101 MHz, CDCl₃) δ : 13.3 (d, J_p = 45.9 Hz), 15.5 (CH₃), 25.6 (d, J_p = 4.0 Hz, 3xCH₃), 28.3 (d, J_p = 2.4 Hz, CH₂), 32.0 (d, J_p = 4.8 Hz, CH), 32.5 (CH₂), 33.8 (CH₂), 36.9 (d, J_p = 30.4 Hz, Cq), 42.4 (CH₂), 62.6 (CH), 82.1 (CH), 82.8 (CH), 88.5 (CH), 92.2 (d, J_p = 16.4 Hz, CH), 96.4 (d, J_p = 9.8 Hz, CH), 117.6 (4xCH), 124.4 (CH), 124.7 (q, J_F = 272.6 Hz, 8xCF₃), 128.5–129.6 (m, 8xCq), 128.8 (Cq), 128.9 (CH), 134.9 (8xCH), 135.0 (CH), 140.9 (CH), 155.7 (d, J_p = 7.0 Hz, Cq), 161.8 (q, J_F = 99.8, 49.9 Hz), 180.7 (Cq)

ppm. ^{31}P NMR (162 MHz, CDCl_3) δ : 50.5 (s) ppm. HRMS (ESI, infusion): calc for $[\text{C}_{24}\text{H}_{37}\text{IrN}_2\text{OP}]^+$: 593.2261, found 593.2258. Calc for $[\text{C}_{32}\text{H}_{12}\text{BF}_{24}]^-$: 863.0660, found 863.0666.

4.9. General procedure for asymmetric hydrogenation

Substrate (1 eq.), the corresponding catalyst (5 mol%) and a PTFE-coated stir-bar were placed in a glass tube inside a stainless steel high pressure reactor, and anhydrous DCM (0.06 M) was added. The reactor was closed and connected to a hydrogen manifold. The connection was purged with vacuum-nitrogen cycles, the valve of the reactor was opened, it was evacuated and then charged at 50 bar of hydrogen pressure. The valve was closed, the hydrogen manifold was unplugged and the mixture was left to stir at room temperature for 24 h. The reactor was then depressurized, the solvent was evaporated and the conversion of the reaction was determined by ^1H NMR. The enantiomeric excess was determined by chiral HPLC analysis of the reaction crude.

4.10. *tert*-Butyl (*R*)-(2-(4-methoxyphenyl)-3-phenylpropyl)carbamate, **7**

Following the hydrogenation GP, using *N*-Boc-(*Z*)-2-(4-methoxyphenyl)-3-phenylallylamine **6** (14.0 mg, 0.04 mmol), catalyst (*S_P*)-**4a** (3.0 mg, $2.06 \cdot 10^{-3}$ mmol) and DCM (0.65 mL). The reaction was stopped after 24 h and gave full conversion. Analysis of the reaction crude by chiral HPLC revealed 98% ee. ^1H NMR (400 MHz, CDCl_3) δ : 1.38 (s, 9H), 2.75–2.95 (m, 2H), 2.95–3.05 (m, 2H), 3.12–3.26 (m, 1H), 3.46–3.60 (m, 1H), 3.78 (s, 3H), 4.32 (br s, 1H), 6.78–6.85 (m, 2H), 6.97–7.07 (m, 4H), 7.13 (t, $J = 7.3$ Hz, 1H), 7.19 (t, $J = 7.3$ Hz, 2H) ppm. HPLC: Chiralpak IA, heptane:EtOH 98:2, 0.5 mL/min, $\lambda = 210$ nm, t_R (*R*) = 18.1 min, t_R (*S*) = 20.4 min.

Declaration of competing interest

The authors declare that they have no known competing financial interests or personal relationships that could have appeared to influence the work reported in this paper.

Data availability

No data was used for the research described in the article.

Acknowledgement

This work was supported by a grant to A.R. and X.V. from FEDER/Ministerio de Ciencia e Innovación (MICINN) (PID2020-115074 GB-I00). IRB Barcelona is the recipient of institutional funding from MICINN through the Centres of Excellence Severo Ochoa Award and from the CERCA Program of the Catalan Government. P. R. thanks Generalitat de

Catalunya for a predoctoral fellowship.

Appendix A. Supplementary data

Supplementary data to this article can be found online at <https://doi.org/10.1016/j.tet.2023.133647>.

References

- [1]. a) A. Vidal-Ferran, A. Grabulosa, X. Verdaguier, A. Riera, *Asymmetric hydrogenation*, in: *Catalytic Asymmetric Synthesis*, 2022, pp. 561–616; b) C.S. G. Seo, R. H. Morris, *Organometallics*, **38** (2018) 47–65. c) P. Etayo, A. Vidal-Ferran, *Chem. Soc. Rev.* **42** (2013) 728–754.
- [2]. A. Cabré, X. Verdaguier, A. Riera, *Chem. Rev.* **122** (2022) 269–339.
- [3]. a) C. Margarita, P.G. Andersson, *J. Am. Chem. Soc.* **139** (2017) 1346–1356; b) J. Johan Verendel, O. Pàmies, M. Diéguez, P.G. Andersson, *Chem. Rev.* **114** (2013) 2130–2169; c) M. Biosca, P. de la Cruz-Sánchez, J. Faiges, J. Margalef, E. Salomó, A. Riera, X. Verdaguier, J. Ferré, F. Maseras, M. Besora, O. Pàmies, M. Diéguez, *ACS Catal.* **13** (2023) 3020–3035.
- [4]. X. Cui, K. Burgess, *Chem. Rev.* **105** (2005) 3272–3296; b) J. Johan Verendel, T. Zhou, J.-Q. Li, A. Paptchikhine, O. Lebedev, P. G. Andersson, *J. Am. Chem. Soc.* **132** (2010) 8880–8881; c) Y. Zhu, S. Khumsubdee, A. Schaefer, K. Burgess, *J. Org. Chem.* **76** (2011) 7449–7457.
- [5]. A.N. Kim, B.M. Stoltz, *ACS Catal.* **10** (2020) 13834–13851.
- [6]. a) E. Salomó, S. Orgué, A. Riera, X. Verdaguier, *Angew. Chem. Int. Ed.* **55** (2016) 7988–7992; b) A. Cabré, X. Verdaguier, A. Riera, *Adv. Synth. Catal.* **361** (2019) 4196–4200; c) E. Salomó, P. Rojo, P. Hernández-Lladó, A. Riera, X. Verdaguier, *J. Org. Chem.* **83** (2018) 4618–4627; d) E. Salomó, A. Gallen, G. Sciortino, G. Ujaque, A. Grabulosa, A. Lledós, A. Riera, X. Verdaguier, *J. Am. Chem. Soc.* **140** (2018) 16967–16970; e) A. Cabré, M. Garçon, A. Gallen, L. Grisoni, A. Grabulosa, X. Verdaguier, A. Riera, *ChemCatChem* **12** (2020) 4112–4120; f) A. Cabré, A. Riera, X. Verdaguier, *Acc. Chem. Res.* **53** (2020) 676–689; g) R. Álvarez-Yebra, P. Rojo, A. Riera, X. Verdaguier, *Tetrahedron* **75** (2019) 4358–4364.
- [7]. P. Rojo, M. Molinari, A. Cabré, C. García-Mateos, A. Riera, X. Verdaguier, *Angew. Chem. Int. Ed.* **61** (2022), e202204300.
- [8]. F. Menges, A. Pfaltz, Pfaltz and co-workers developed the ligand ThrePHOX derived from threonine, *Adv. Synth. Catal.* **344** (2002) 40–44.
- [9]. S. Nanchen, A. Pfaltz, Some years ago, Pfaltz and co-workers reported the cyclometallation of an *N*-heterocyclic carbene-oxazoline ligand, *Chem. Eur. J.* **12** (2006) 4550–4558 (In that case, only the cyclometallated complex was isolated).
- [10]. Crystallographic data (excluding structure factors) for the structure in this paper has been deposited with the Cambridge Crystallographic Data Centre as supplementary publication no. CCDC 2270887. Copies of the data can be obtained, free of charge, on application to CCDC, 12 Union Road, Cambridge CB2 1EZ, UK, (fax: +44-(0)1223-336033 or e-mail: deposit@ccdc.cam.ac.uk).
- [11]. The same geometry is observed for the cyclometallated complex reported by Pfaltz and co-workers (ref 9).
- [12]. We attribute the conversions and selectivity differences between (*R_P*)-**4a** and (*R_P*)-**5a** to the temperature gradient of the reaction vessel upon initial heating to 80 °C. For (*R_P*)-**4a**, since no equilibration is needed for activation, hydrogenation is likely to occur to a large extent at lower temperature, before reaching 80 °C.
- [13]. a) S. Orgué, A. Flores, M. Biosca, O. Pàmies, M. Diéguez, A. Riera, X. Verdaguier, *Chem. Commun.* **51** (2015) 17548–17551; b) E. Salomó, A. Prades, A. Riera, X. Verdaguier, *J. Org. Chem.* **82** (2017) 7065–7069.